전산공력음향학을 위한 적응형 비선형 인공감쇄모형

Adaptive Nonlinear Artificial Dissipation Model for Computational Aeroacoustics

김 재 욱*, 이 덕 주
Jae Wook Kim and Duck Joo Lee

한국과학기술원 기계공학과 항공우주공학전공

An adaptive nonlinear artificial dissipation model is presented for performing aeroacoustic computations by the high-order and high-resolution numerical schemes based on the central finite differences. An effective formalism of it is devised by combining a selective background smoothing term and a well-established nonlinear shock-capturing term, which is for the temporal accuracy as well as the numerical stability. A conservative form of the selective background smoothing term is presented to keep accurate phase speeds of the propagating nonlinear waves. The nonlinear shock-capturing term that has been modeled by the second-order derivative term is combined with it to improve the resolution of discontinuities and stabilize the strong nonlinear waves. It is shown that the improved artificial dissipation model with an adaptive control constant which is independent of problem types reproduces the correct profiles and speeds of nonlinear waves, suppresses numerical oscillations near discontinuity and avoids unnecessary damping on the smooth linear acoustic waves. The feasibility and performance of the adaptive nonlinear artificial dissipation model are investigated by the applications to actual computational aeroacoustics pro blems.

I. Introduction

The high-order and high-resolution numerical schemes based on the central finite differences [1-3] have been developed for computational aeroacoustics (CAA) so far and these are well adapted for the linear wave solutions. These are properly formulated to be less dissipative and dispersive than the other low-order standard schemes. These can reproduce the wave profile and speed accurately using less than several grid points per wavelength. On the other hand, it has been generally recognized that these are less suitable for the computation of nonlinear wave solutions, especially when discontinuities such as shocks or contact surfaces are present. Nonlinearity causes the wave profile of an acoustic pulse to steepen up and ultimately to form a shock. It was found that the nonlinear wave steepening process, when viewed in the wavenumber domain, corresponded to an energy cascade process whereby low wavenumber components are transferred to high wavenumber range [4]. When shocks are formed, it is known that these generally produce spurious spatial oscillations around them and in regions with steep gradients. These spurious oscillations are waves from the unresolved high wavenumber range generated by the nonlinear wave cascading process. If the high-order and high-resolution schemes based on the central differences are used for the nonlinear computation without an artificial dissipation model, the computed nonlinear wave profile remains accurate as long as the cascading process does not transfer wave components into the unresolved narrow band of high wavenumber range.

Several kinds of artificial dissipation models were developed so far for the purpose of obtaining numerical stability and efficient convergence features of numerical schemes based on the central differences [5-11]. These present good resolution characteristics near discontinuity of nonlinear waves but have a tendency to damp out the amplitude of linear waves seriously, because these were originally designed to suppress the low wavenumber components of a wave profile. Therefore these are not suited for the time-accurate numerical solutions of aeroacoustic problems that contain linear waves of very small amplitudes in the far field. Jameson [5], Pulliam [6] and others [7-9] applied the nonlinear artificial dissipation model to the steady Euler computations, which was a blend of the second-order and fourth-order derivative term with the nonlinear switching coefficients. It has excellent shock-capturing properties and helps fast convergence to the steady state, but it leads to the unnecessary damping on the linear waves because it cannot distinguish the small-amplitude linear waves from the spurious numerical oscillations. The artificial selective damping model was introduced by Tam et al. [10, 11] to solve the nonlinear acoustic problems using the dispersion-relation-preserving scheme [12] which is a high-order and high-resolution solver based on the central differences. The artificial selective damping model has been used for time-dependent CAA solutions and not for the convergence to a steady-state solution. It was designed to damp out the spurious wave components effectively in the high wavenumber range unresolved by the finite difference scheme, while at the same time keeping the wave components in a wide band of the low wavenumber range unaffected. It is good for linear waves without unnecessary damping, however it lacks the shock-capturing properties to resolve the nonlinear discontinuity and is not able to remove the spurious oscillations sufficiently around the nonlinear waves.

In this paper, an improved formulation of artificial dissipation model is derived for CAA, which removes the spurious numerical oscillations produced by the nonlinear waves completely but does not have an effect on the linear waves. The artificial selective damping model and the nonlinear artificial dissipation model are combined for the numerical stability and temporal accuracy of CAA performed by the high-order and high-resolution central difference schemes. The artificial selective damping model is reformulated into a conservative form to maintain the correct phase speeds of nonlinear waves. The second-order de-

rivative term in the nonlinear artificial dissipation model is combined with the artificial selective damping model to improve the shock-capturing property progressively. Multi-dimensional formalism is presented in the generalized coordinates for practical applications to the problems with complex geometry. An adaptive constant is devised to control the local magnitude of dissipation level automatically and need not be readjusted for a variety of problems. Therefore the new model is developed as an adaptive nonlinear artificial dissipation model. The accuracy of adaptive nonlinear artificial dissipation model is verified by the simple one-dimensional computations on the linear wave convection and shock tube simulation problem that have the exact solutions. Its results are compared with those of the artificial selective damping model (Tam et al.'s) and the nonlinear artificial dissipation model (Jameson et al.'s). It is also applied to the quasi-one-dimensional and two-dimensional computations of propagating sound waves through a shock in a transonic nozzle. The compressible Euler equations in the conservative form are solved for these computations. The feasibility and performance of the adaptive nonlinear artificial dissipation model are investigated for CAA in the present paper.

II. Governing Equations

The unsteady compressible Euler equations in the conservative form are considered for the formulation of artificial dissipation models and their applications to actual computations in the present work. One-dimensional equations in Cartesian coordinates, quasi-one-dimensional and two-dimensional equations in the generalized coordinates are considered.

1-D Equations

The one-dimensional Euler equations in Cartesian coordinates are expressed in a flux vector form as

$$\frac{\partial \mathbf{Q}}{\partial t}+\frac{\partial \mathbf{E}}{\partial x}=\mathbf{0} \tag{1}$$

where Q is the vector of conservative variables and E is the inviscid flux vector. These vectors are given by

$$\mathbf{Q}=[\rho,\rho u,\rho e_t]^T,\quad \mathbf{E}=[\rho u,\rho u^2+p,(\rho e_t+p)u]^T$$

where the total internal energy e_t is defined as

$$e_t=p/[(\gamma-1)\rho]+u^2/2.$$

Quasi-1-D Equations

The quasi-one-dimensional Euler equations in the generalized coordinates are expressed in a flux vector form as

$$\frac{\partial(A\hat{\mathbf{Q}})}{\partial t}+\frac{\partial(A\hat{\mathbf{E}})}{\partial \xi}-\hat{\mathbf{H}}=\mathbf{0} \tag{2}$$

where $\hat{\mathbf{Q}}$ is the vector of conservative variables, $\hat{\mathbf{E}}$ is the inviscid flux vector and $\hat{\mathbf{H}}$ is the source vector in the generalized coordinate system. $A = A(x)$ is the cross-sectional area. The superscript '$\wedge$' denotes the functions in the generalized coordinates system. These vectors are given as

$$\hat{\mathbf{Q}}=\mathbf{Q}/J,\quad \hat{\mathbf{E}}=\xi_x\mathbf{E}/J,\quad \hat{\mathbf{H}}=\frac{dA}{d\xi}[0,p,0]^T/J$$

where J is the transformation Jacobian and ξ_x is the transformation metric from the Cartesian to the generalized coordinates. In the one-dimensional case, J equals to ξ_x.

2-D Equations

For a practical computation in a domain with complex geometry or boundaries, it is necessary to utilize the multi-dimensional equations that are transformed from a physical space with Cartesian coordinates to a computational space with the generalized coordinates. The two-dimensional Euler equations in the generalized coordinates are expressed in a flux vector form as

$$\frac{\partial \hat{\mathbf{Q}}}{\partial t}+\frac{\partial \hat{\mathbf{E}}}{\partial \xi}+\frac{\partial \hat{\mathbf{F}}}{\partial \eta}=\mathbf{0} \tag{3}$$

where the vector of conservative variables and the inviscid flux vectors are given as

$$\hat{\mathbf{Q}}=[\rho,\rho u,\rho v,\rho e_t]^T/J,$$

$$\hat{\mathbf{E}}=[\rho U,\rho uU+\xi_x p,\rho vU+\xi_y p,(\rho e_t+p)U]^T/J,$$

$$\hat{\mathbf{F}}=[\rho V,\rho uV+\eta_x p,\rho vV+\eta_y p,(\rho e_t+p)V]^T/J.$$

The superscript '$\wedge$' denotes the functions in the generalized coordinates system. J is the transformation Jacobian, ξ_x, ξ_y, η_x and η_y are the transformation metrics from Cartesian to the generalized coordinates in two dimensions. The contravariant velocities U and V are expressed as

$$U=\xi_x u+\xi_y v,\quad V=\eta_x u+\eta_y v.$$

The total internal energy in two dimensions is defined as

$$e_t=p/[(\gamma-1)\rho]+(u^2+v^2)/2.$$

III. Previous Artificial Dissipation Models

It has been shown that the artificial dissipation terms introduce an upwind correction to the central difference schemes, such as to remove non-physical effects arising from the central discretization of wave propagation phenomena. These effects arise mainly around the discontinuities, where a sudden change in the propagation direction of certain waves occurs. Due to its nature, the central discretization is not able to handle this discontinuous change and generates oscillations. Therefore, in the early stage, the artificial dissipation models had been developed to remove the spurious oscillations, which was for the robustness of stability and fast convergence of solutions in the steady-state aerodynamics sense. Recently, the focus of artificial dissipation model was changed to the accurate computations of unsteady aerodynamics in the near field and, especially, acoustics in the far field.

Nonlinear Artificial Dissipation Model

The artificial viscosity or artificial dissipation models have been developed so far for the purpose of achieving fast convergence to steady-state solutions without the unavoid-

able high-frequency oscillations around discontinuities. These additional terms should simulate the effects of the physical viscosity on the scale of the grid mesh locally around the discontinuities and be negligible, that is of an order equal or higher than the truncation error, in smooth regions [12]. Jameson et al. have employed the nonlinear artificial dissipation model which consists of the second-order and fourth-order derivative term with excellent shock-capturing properties. In this approach the fourth-order derivative term is switched off when the pressure gradient dominates. Consider an one-dimensional equation of fluid motion, i.e. compressible Euler equation discretized on a uniform grid mesh with spacing Δx. Suppose the dissipation term added to the right side of the Eq. (1), which consists of the values of a conservative variable in the finite difference stencil. At the i-th grid point, Euler equations with the nonlinear artificial dissipation term D_i can be written as

$$\left.\frac{\partial \mathbf{Q}}{\partial t}\right|_i + \left.\frac{\partial \mathbf{E}}{\partial x}\right|_i = \mathbf{D}_i \,. \tag{4}$$

The artificial dissipation term, D_i is represented by the difference of the numerical dissipation flux vector, $\mathbf{d}_i$:

$$\mathbf{D}_i = \left(\mathbf{d}_{i+\frac{1}{2}} - \mathbf{d}_{i-\frac{1}{2}}\right)/\Delta x \,, \tag{5}$$

$$\mathbf{d}_{i+\frac{1}{2}} = |\lambda|_{i+\frac{1}{2}}\left[\varepsilon^{(2)}_{i+\frac{1}{2}}(\mathbf{Q}_{i+1} - \mathbf{Q}_i) - \varepsilon^{(4)}_{i+\frac{1}{2}}(\mathbf{Q}_{i+2} - 3\mathbf{Q}_{i+1} + 3\mathbf{Q}_i - \mathbf{Q}_{i-1})\right] \tag{6}$$

Equation (5) and (6) express the combination of the second-order and fourth-order derivative term with local nonlinear dissipation functions and absolute eigenvalue. The absolute eigenvalue and its midpoint value are as follows:

$$|\lambda|_i = (|u| + c)_i \,, \tag{7}$$

$$|\lambda|_{i+\frac{1}{2}} = (|\lambda|_i + |\lambda|_{i+1})/2 \,. \tag{8}$$

where u is the flow velocity in x-direction and c is the speed of sound. The nonlinear dissipation function $\varepsilon^{(2)}$ is evaluated as follows:

$$\varepsilon^{(2)}_i = \kappa^{(2)}\,|p_{i+1} - 2p_i + p_{i-1}|/(p_{i+1} + 2p_i + p_{i-1}) \,, \tag{9}$$

$$\varepsilon^{(2)}_{i+\frac{1}{2}} = \max\left(\varepsilon^{(2)}_i, \varepsilon^{(2)}_{i+1}\right), \tag{10}$$

where $\kappa^{(2)}$ is an adjustable constant and p is the pressure. The pressure term in $\varepsilon^{(2)}$ is generally of second order, except in regions of strong pressure gradients, where it reduces to first order or becomes of the order of one. Hence, around shocks, the $\varepsilon^{(2)}$ term is dominating. This did not appear to be sufficient to avoid completely some small oscillations, of the order of one per cent in density variation, preventing the complete convergence to the steady state. These oscillations were removed by introducing the fourth-order derivative term, providing some background dissipation through the domain, but led to the reappearance of overshoots around the shock waves. Therefore, the background dissipation is turned off when $\varepsilon^{(2)}$ is large and one defines

$$\varepsilon^{(4)}_{i+\frac{1}{2}} = \max\left[0\,,\left(\kappa^{(4)} - \varepsilon^{(2)}_{i+\frac{1}{2}}\right)\right] \tag{11}$$

where $\kappa^{(4)}$ is an adjustable constant. The typical values of $\kappa^{(2)} = 1/2$ and $\kappa^{(4)} = 1/100$ suggested by Jameson et al. are used for the optimal results in the present computations. This model has excellent shock-capturing features and gives sufficient numerical stability to the central difference schemes. However, it was not designed for the time-dependent solutions of aeroacoustic problems, the excessive dissipation occurs in the low wavenumber range and the linear acoustic waves might be suppressed seriously.

Artificial Selective Damping Model

To obtain a high-quality numerical solution, it is necessary to eliminate the spurious numerical wave components in the narrow band of high wavenumber range, while at the same time keeping the wave components in the wide band of low wavenumber range unaffected. This can be achieved by inserting the artificial selective damping terms that is introduced by Tam et al. in the finite difference equations. It is constructed in the seven-point stencil as suggested in Ref. 10 and 11, and it can be written here as

$$\mathbf{D}_i = -\frac{\nu_a}{(\Delta x)^2}\sum_{m=-3}^{3} a_m \mathbf{Q}_{i+m} \tag{12}$$

where ν_a is an variable artificial viscosity to determine the magnitude of damping and a_m's are the damping coefficients. The damping coefficients a_m's are determined by the Fourier analysis in the wavenumber domain. By choosing the coefficients properly, it can be possible to make the damping occur only in the narrow band of high wavenumber range and the way to optimize them is represented precisely in Ref. 2, 10 and 11. The authors suggest these coefficients as follows:

$a_0 = 0.3248765149154926,$
$a_1 = a_{-1} = -0.2355295710360009,$
$a_2 = a_{-2} = 0.08756174254225371,$
$a_3 = a_{-3} = -0.01447042896399915.$

The variable artificial viscosity was defined as

$$\nu_a = u_i^{\text{stencil}}\Delta x / Re_a \tag{13}$$

where the stencil velocity is given as

$$u_i^{\text{stencil}} = \max_{m=-3}^{3}(u_{i+m}) - \min_{m=-3}^{3}(u_{i+m}) \,. \tag{14}$$

Then the artificial selective damping term is rewritten as

$$\mathbf{D}_i = -\frac{u_i^{\text{stencil}}}{Re_a \Delta x}\sum_{m=-3}^{3} a_m \mathbf{Q}_{i+m} \,. \tag{15}$$

The stencil velocity is for measuring the velocity gradient or shock strength in the seven-point stencil and Re_a is an artificial Reynolds number to control the overall magnitude of damping. The typical value of $Re_a \approx 0.05$ suggested by Tam et al. is used for the optimal results in the present computations. The stencil velocity defined in Eq. (14) is a function of space, whose value varies with the grid points. It is not contained in the difference operator as shown in Eq. (15), thus it produces a non-conservative feature of the artificial selective damping model. It makes some error in the phase speeds of the propagating nonlinear waves. The artificial selective damping model is good for suppressing the undesirable spurious oscillations in entire computational domain. However, it cannot help generating unavoidable oscillations locally when it meets a strong discontinuity, because it has no shock-capturing term to be switched on in such a case. The amplitude of these oscillations does not seem so high but, in many cases, these can result in a serious problem to be handled carefully.

IV. Adaptive Nonlinear Artificial Dissipation (ANAD) Model

The classical artificial dissipation consists of the second-order and fourth-order derivative term in conservative form. The former is for shock-capturing feature and the latter is for background smoothing effect. But the effect of the background smoothing term is so excessive that it may damp out the linear acoustic waves seriously and it is not proper for CAA. On the other hand, the artificial selective damping model lacks a stability to capture a high discontinuity generated from a strong nonlinear wave and still produces numerical oscillations near the discontinuity. It was proposed in a non-conservative form so it may have some error in reproducing the phase speeds of nonlinear waves if it is used in the original form. In this paper, a revised formulation of the artificial selective damping term in conservative form is presented. Then, it is desirable to combine the shock-capturing term and the artificial selective damping term as the background smoothing term. In this paper, this combination supported by an adaptive control constant and nonlinear switching functions is proposed as an adaptive nonlinear artificial dissipation (ANAD) model.

Conservative Form of Background Smoothing Term

It is required to confine the variable that is a space function within the difference operator so as to construct a conservative formulation. In Eq. (15), the stencil velocity is out of the damping operator and the formulation is not conservative yet. Therefore the damping operator should be changed into a difference operator of two split damping flux terms and each flux term should include the stencil velocity. Then the background smoothing term is represented in the conservative form as

$$\mathbf{D}_i = \left(\mathbf{d}_{i+\frac{1}{2}} - \mathbf{d}_{i-\frac{1}{2}}\right)/\Delta x \tag{16}$$

and the damping flux vector, $\mathbf{d}_i$ is given as

$$\mathbf{d}_{i+\frac{1}{2}} = C_{i+\frac{1}{2}} \sum_{m=-2}^{3} b_m \mathbf{Q}_{i+m} \,. \tag{17}$$

where the $C_{i+\frac{1}{2}}$ is a controlling function of dissipation magnitude at the interface of adjacent two cell's. It is given as $C_{i+\frac{1}{2}} = -u^{\text{stencil}}_{i+\frac{1}{2}} / Re_a$ for Tam et al.'s model described in Eq. (15), and it is changed to an improved form for ANAD model in this paper as will be shown in the next subsections. The equation (16) is of the flux difference form and all the space functions are confined within the difference operator, i.e. the conservative form is achieved. The damping coefficients b_m's are determined by some arithmetic relations matching with the coefficients a_m's in Eq. (15). The matching condition makes Eq. (16) equal to Eq. (15) when the stencil velocity is not a variable locally, and it is represented as

$$\sum_{m=-2}^{3} b_m \mathbf{Q}_{i+m} - \sum_{m=-2}^{3} b_m \mathbf{Q}_{(i-1)+m} = \sum_{m=-3}^{3} a_m \mathbf{Q}_{i+m} \,. \tag{18}$$

The equation (18) should be satisfied independently of the location or the index 'i' of the grid points. In this course, the following relation is derived for the determination of the new damping coefficients:

$$b_m = \sum_{n=m}^{3} a_n \quad (m = -2, \cdots, 3) \tag{19}$$

then the coefficients are obtained as follows:

$b_1 = -b_0 = -0.1624382574577463$,
$b_2 = -b_{-1} = 0.07309131357825455$,
$b_3 = -b_{-2} = -0.01447042896399915$.

Using the above coefficients, the conservative formulation of the artificial selective damping model is achieved, which is used as the background smoothing term in the present paper. The effect of conservative formulation is compared with that of non-conservative one, by their application to actual computations in Section V.

1-D Formulation of ANAD Model

The ANAD model is presented by combining the shock-capturing term in Eq. (6) and the background smoothing term in Eq. (17) with modified nonlinear dissipation functions. One-dimensional formalism of ANAD model is suggested in Cartesian coordinates. Consider the dissipation term D_i included in Eq. (1) at the i-th grid point as expressed in Eq. (4), where the dissipation term is represented in the conservative form as

$$\mathbf{D}_i = \left(\mathbf{d}_{i+\frac{1}{2}} - \mathbf{d}_{i-\frac{1}{2}}\right)/\Delta x \tag{20}$$

which is the same as Eq. (5), then the numerical dissipation flux vector is revised in this paper as

$$\mathbf{d}_{i+\frac{1}{2}} = |\lambda|^{\text{stencil}}_{i+\frac{1}{2}} \left[\varepsilon^{(2)}_{i+\frac{1}{2}} (\mathbf{Q}_{i+1} - \mathbf{Q}_i) - \varepsilon^{(4)}_{i+\frac{1}{2}} \sum_{m=-2}^{3} b_m \mathbf{Q}_{i+m} \right]. \tag{21}$$

Equation (20) and (21) express the combination of the second-order and the fourth-order derivative term with the local nonlinear dissipation functions and the stencil eigenvalue. The stencil eigenvalue is evaluated on the midpoint just like the stencil velocity in Eq. (18) and it is used as the shock or discontinuity detector measuring the slope or gradient of primitive variables. It is represented as

$$|\lambda|^{\text{stencil}}_{i+\frac{1}{2}} = \max_{m=-2}^{3}(|\lambda|_{i+m}) - \min_{m=-2}^{3}(|\lambda|_{i+m}) \tag{22}$$

where the absolute eigenvalue is defined in Eq. (7). The nonlinear dissipation functions, $\varepsilon^{(2)}$ and $\varepsilon^{(4)}$ in Eq. (21) determine magnitudes of the second-order dissipation and the fourth-order dissipation according to the change of pressure gradient. In regions of strong discontinuity, the second-order dissipation, i.e. the shock-capturing term dominates and the fourth-order one is turned off. Out of the region, the second-order one becomes very small value and the fourth-order one, i.e. the background smoothing term governs the dissipation. The nonlinear dissipation functions are suggested in this paper as

$$\varepsilon^{(2)}_{i+\frac{1}{2}} = \kappa \max_{m=-2}^{3}(\nu_{i+m}), \tag{23}$$

$$\varepsilon^{(4)}_{i+\frac{1}{2}} = \max\left[0, \left(\kappa - \varepsilon^{(2)}_{i+\frac{1}{2}}\right)\right], \tag{24}$$

where the shock detector, ν_i is given as

$$\nu_i = |p_{i-1} - 2p_i + p_{i+1}| / (p_{i-1} + 2p_i + p_{i+1}) \,.$$

Equation (23) is extended from Eq. (10) for the purpose of having an effect on the wide stencil of high-order and high-resolution schemes in the present paper. The adaptive control constant, κ is devised in this paper to determine the

magnitude of dissipation level in entire domain and this is automatically adjusted according to the flow conditions or problem types. The adaptive control constant is evaluated as

$$\kappa = \left[\frac{\alpha+1}{\alpha-1}\tanh(\alpha-1)\right]^{1+\tanh(\sigma-1)} \Big/ \sigma^{1/\alpha} \qquad (25)$$
$$\sigma = p^{max}/p^{min}, \quad \alpha = |\lambda|^{max}/|\lambda|^{min}$$

where the superscripts, 'max' and 'min' imply the maximum and minimum value of the variable along a grid line, respectively, which are expressed as

$$f^{max} = \max_{i=0}^{imax} f_i, \quad f^{min} = \min_{i=0}^{imax} f_i. \qquad (26)$$

The adaptive control constant expressed in Eq. (25) is newly suggested in this paper for effective applications of the artificial dissipation model to various CAA problems in one-dimensional Cartesian coordinates, which can be used for the linear and nonlinear waves at once. At each time step, the optimal value of the control constant is calculated automatically by the flow properties. One need not readjust the constant according to case-by-case nor waste additional computation time to find out an optimal value of it.

Quasi-1-D Formulation of ANAD Model

Quasi-one-dimensional formalism of ANAD model is suggested in the generalized coordinates. Consider the dissipation term added on the right hand side of the quasi-one-dimensional Euler equations expressed by Eq. (2) at the i-th grid point:

$$\left.\frac{\partial(A\hat{\mathbf{Q}})}{\partial t}\right|_i + \left.\frac{\partial(A\hat{\mathbf{E}})}{\partial \xi}\right|_i - \hat{\mathbf{H}}_i = \hat{\mathbf{D}}_i \qquad (27)$$

where the dissipation term $\hat{\mathbf{D}}_i$ is given as

$$\hat{\mathbf{D}}_i = \left(A_{i+\frac{1}{2}}\hat{\mathbf{d}}_{i+\frac{1}{2}} - A_{i-\frac{1}{2}}\hat{\mathbf{d}}_{i-\frac{1}{2}}\right)\Big/\Delta\xi. \qquad (28)$$

Then the numerical dissipation flux vector in the generalized coordinates is given in this paper as

$$\hat{\mathbf{d}}_{i+\frac{1}{2}} = |\lambda|^{stencil}_{i+\frac{1}{2}}\left[\varepsilon^{(2)}_{i+\frac{1}{2}}(\mathbf{Q}_{i+1}-\mathbf{Q}_i) - \varepsilon^{(4)}_{i+\frac{1}{2}}\sum_{m=-2}^{3} b_m \mathbf{Q}_{i+m}\right]\Big/ J_{i+\frac{1}{2}}. \qquad (29)$$

The cross-section area on the midpoint in Eq. (28) and the transformation Jacobian on the midpoint in Eq. (29) are evaluated just by the arithmetic averages of their values on the adjacent two grid points as

$$A_{i+\frac{1}{2}} = (A_{i+1}+A_i)/2, \quad J_{i+\frac{1}{2}} = (J_{i+1}+J_i)/2.$$

The stencil eigenvalue, $|\lambda|^{stencil}_{i+\frac{1}{2}}$ is evaluated also by Eq. (22) in this case, where the absolute eigenvalue, $|\lambda|_i$ is defined differently compared with Eq. (7) in the generalized coordinates as

$$|\lambda|_i = (|u|+c)_i|\xi_x|_i.$$

The nonlinear dissipation functions, $\varepsilon^{(2)}_{i+\frac{1}{2}}$, $\varepsilon^{(4)}_{i+\frac{1}{2}}$ and the shock detector, ν_i are the same as those of one-dimensional case expressed above. The adaptive control constant in the generalized coordinates is also devised in this paper as

$$\kappa = \left[1+(\sigma-1)\tanh\left(\frac{\alpha}{\beta}-1\right)\right]\left(\sqrt{\hat{\alpha}\hat{\beta}}\right)^{1+\tanh(\sigma-1)} \Big/ \sigma^{R}, \qquad (30)$$

$$\sigma = p^{max}/p^{min}, \quad \alpha = |\lambda|^{max}/|\lambda|^{min},$$
$$\beta = (|\lambda|/|\xi_x|)^{max}/(|\lambda|/|\xi_x|)^{min}, \quad R = (\alpha+\beta)/(2\alpha\beta),$$
$$\hat{\alpha} = \frac{\alpha+1}{\alpha-1}\tanh(\alpha-1), \quad \hat{\beta} = \frac{\beta+1}{\beta-1}\tanh(\beta-1).$$

where the meanings of the superscripts, 'max' and 'min' are explained by Eq. (26). The adaptive control constant expressed in Eq. (30) is for one-dimensional generalized coordinate.

2-D Formulation of ANAD Model

For a practical computation in a domain with complex geometry of boundaries, it is necessary to utilize the multi-dimensional equations that are transformed from a physical space with Cartesian coordinates to a computational space with the generalized coordinates. Two-dimensional formalism of ANAD model is suggested in the generalized coordinates. Consider the dissipation model added on the right hand side of the two-dimensional Euler equations expressed by Eq. (3), where the dissipation model is divided into two terms in the ξ-direction and η-direction. The equations with the two ANAD terms are written at the (i,j)-th grid point as

$$\left.\frac{\partial\hat{Q}}{\partial t}\right|_{i,j} + \left.\frac{\partial\hat{E}}{\partial\xi}\right|_{i,j} + \left.\frac{\partial\hat{F}}{\partial\eta}\right|_{i,j} = \hat{\mathbb{D}}^{\xi}_{i,j} + \hat{\mathbb{D}}^{\eta}_{i,j} \qquad (31)$$

where $\hat{\mathbb{D}}^{\xi}_{i,j}$ is the dissipation term in the ξ-direction and $\hat{\mathbb{D}}^{\eta}_{i,j}$ is that in the η-direction. The ANAD term in the ξ-direction is represented in the finite difference form as

$$\hat{\mathbb{D}}^{\xi}_{i,j} = \left(\hat{\mathbb{d}}^{\xi}_{i+\frac{1}{2},j} - \hat{\mathbb{d}}^{\xi}_{i-\frac{1}{2},j}\right)\Big/\Delta\xi \qquad (32)$$

where the numerical dissipation flux is

$$\hat{\mathbb{d}}^{\xi}_{i+\frac{1}{2},j} = |\lambda|^{stencil}_{i+\frac{1}{2},j}\left[\varepsilon^{(2)}_{i+\frac{1}{2},j}(\mathbb{Q}_{i+1,j}-\mathbb{Q}_{i,j}) + \varepsilon^{(4)}_{i+\frac{1}{2},j}\sum_{m=-2}^{3} b_m \mathbb{Q}_{i+m,j}\right]\Big/ J_{i+\frac{1}{2},j} \qquad (33)$$

The two-dimensional stencil eigenvalue is defined as

$$|\lambda|^{stencil}_{i+\frac{1}{2},j} = \max_{m=-2}^{3}(|\lambda|_{i+m,j}) - \min_{m=-2}^{3}(|\lambda|_{i+m,j}).$$

The two-dimensional absolute eigenvalue is expressed in the generalized coordinates as

$$|\lambda|_{i,j} = \left(|U| + c\sqrt{\xi_x^2+\xi_y^2}\right)_{i,j}.$$

The two-dimensional transformation Jacobian on the midpoint in Eq. (33) is evaluated just by the arithmetic averages of their values on the adjacent two grid points as

$$J_{i+\frac{1}{2},j} = (J_{i+1,j}+J_{i,j})/2.$$

The nonlinear dissipation functions and the shock detector in this case are the same as those of the one-dimensional or the quasi-one-dimensional case but expressed in the two-dimensional notations as follows:

$$\varepsilon^{(2)}_{i+\frac{1}{2},j} = \kappa_j \max_{m=-2}^{3}(\nu_{i+m,j}), \quad \varepsilon^{(4)}_{i+\frac{1}{2},j} = \max\left[\left(\kappa_j - \varepsilon^{(2)}_{i+\frac{1}{2},j}\right), 0\right],$$
$$\nu_{i,j} = \left|p_{i-1,j} - 2p_{i,j} + p_{i+1,j}\right| \Big/ \left(p_{i-1,j} + 2p_{i,j} + p_{i+1,j}\right).$$

The adaptive control constant in this case is the same as that of the quasi-one-dimensional case in the generalized coordinates but expressed in the two-dimensional notations as

$$\kappa_j = \left[1+(\sigma_j-1)\tanh\left(\frac{\alpha_j}{\beta_j}-1\right)\right]\left(\sqrt{\hat{\alpha}_j\hat{\beta}_j}\right)^{1+\tanh(\sigma_j-1)} \Big/ \sigma_j^{R_j}, \quad (34)$$

$$\sigma_j = p_j^{\max}/p_j^{\min}, \quad \alpha_j = |\lambda|_j^{\max}/|\lambda|_j^{\min},$$

$$\beta_j = \left(|\lambda|\sqrt{\xi_x^2+\xi_y^2}\right)_j^{\max} \Big/ \left(|\lambda|\sqrt{\xi_x^2+\xi_y^2}\right)_j^{\min}, \quad R_j = (\alpha_j+\beta_j)/(2\alpha_j\beta_j),$$

$$\hat{\alpha}_j = \frac{\alpha_j+1}{\alpha_j-1}\tanh(\alpha_j-1), \quad \hat{\beta}_j = \frac{\beta_j+1}{\beta_j-1}\tanh(\beta_j-1).$$

where the superscripts, 'max' and 'min' imply the maximum and minimum value of the variable along a grid line, respectively, which are expressed in two dimensions as

$$f_j^{\max} = \max_{i=0}^{imax} f_{i,j}, \quad f_j^{\min} = \min_{i=0}^{imax} f_{i,j}.$$

The adaptive control constant expressed in Eq. (34) is for two-dimensional generalized coordinates. The feasibility of the adaptive control constant is investigated by various numerical experiments using with the high-order and high-resolution schemes in the next section.

V. Application to Computations and Validation

In this section, the ANAD (adaptive nonlinear artificial dissipation) model presented in this paper is applied to actual computations of the benchmarking problems and its accuracy and performance are investigated. One-dimensional linear wave convection and shock-tube simulating problem that have the exact solutions are solved for the comparisons of the present ANAD model and the other models developed previously. Sound wave propagation through a shock in a transonic nozzle is computed as a quasi-one-dimensional problem and the numerical solutions are compared with the analytic solutions. This problem is also solved in two dimensions to validate the two-dimensional ANAD model in the generalized coordinates and its results are compared with those of the quasi-one-dimensional computations. In this course, it is shown the ANAD model enables the central difference schemes to simulate the shock-sound interactions successfully. The feasibility of the ANAD model for linear and nonlinear CAA is testified.

Numerical Schemes and Boundary Conditions

The high-order and high-resolution numerical methods developed for CAA are used in the present computations. The optimized fourth-order compact scheme [1-3] that is a kind of Padé scheme in a pentadiagonal family is used for the evaluation of spatial derivatives. The classical fourth-order Runge-Kutta scheme is used for the temporal integration of solutions. These schemes have the high-resolution characteristics, therefore these can resolve wider band of wavenumber or frequency range than the other well-established low-order ones. However, since the present schemes do not always resolve effectively the high wavenumber or frequency range, the ANAD model could be introduced to remove the unwanted numerical oscillations that may develop.

Besides the stringent requirements on the high-order and high-resolution numerical schemes that are mentioned above, the accurate and robust calculation of sound depends heavily on the suppression of any waves that could result from unwanted reflections on the computational boundaries. Therefore the boundary conditions for CAA should be physically correct and numerically well posed. The generalized characteristic boundary conditions [13-15] are used as that kind of time-dependent boundary conditions in the present computations. The non-reflecting inflow/outflow conditions and transparent source conditions are implemented on the inlet or exit plane [16]. The slip wall conditions are imposed on the wall surfaces in the two-dimensional problem [15].

1-D Computations

For one-dimensional computations, two kinds of initial-value problems are solved; one is the linear wave pulse propagation and the other is the shock-tube simulation. The one-dimensional Euler equations expressed as Eq. (1) are solved. The computation of the first problem starts from the initial conditions that consist of the bell-shaped linear pulses of the density, pressure and velocity, whose magnitudes are equally 1×10^{-4} times of the ambient density, pressure and sound speed, respectively. The second problem starts from the initial conditions that have the discontinuity at the diaphragm where the ratio of values before and behind the diaphragm is 10 : 1 for density and 8.6618 : 0.5 for pressure. In the computations, the accuracy and effectiveness of the ANAD model are studied and compared with the other artificial dissipation models (Jameson et al.'s and Tam et al.'s). The numerical solutions are represented in comparison with the analytic solutions. The results of computations are presented in Fig. 1 and 2.

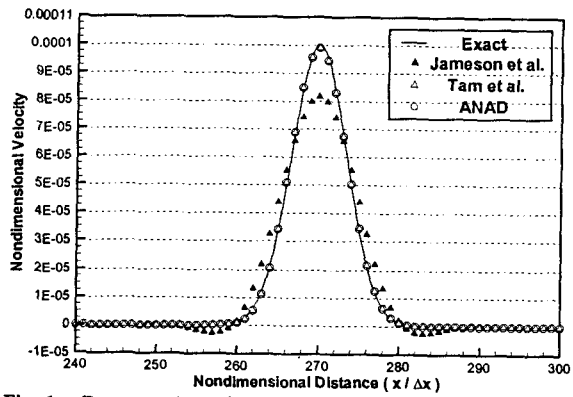

Fig. 1. Computation of linear wave pulse propagation (velocity profile) by: (a) Jameson et al.'s model, (b) Tam et al.'s model, and (c) ANAD model.

In Fig. 1, it is shown that the ANAD model has little effect on the linear wave with very small amplitude and retains the wave profile correctly and similar results are obtained by Tam et al.'s model, while Jameson et al.'s model damps out the linear wave seriously. In Fig. 2, it is shown that the ANAD model captures the strong shock wave and the contact discontinuity with large amplitudes without spurious oscillations and the phase speeds of waves are re-

produced correctly in comparison with analytic solutions, while Jameson et al.'s model makes serious damping on the contact discontinuity and Tam et al.'s model lacks the shock capturing feature, produces spurious oscillations near the shock and makes some error of the nonlinear shock speed. The ANAD model is superior to the other previous artificial dissipation models in all cases. By the results, it is concluded that the ANAD model developed in this paper can be used accurately and effectively for unsteady CAA.

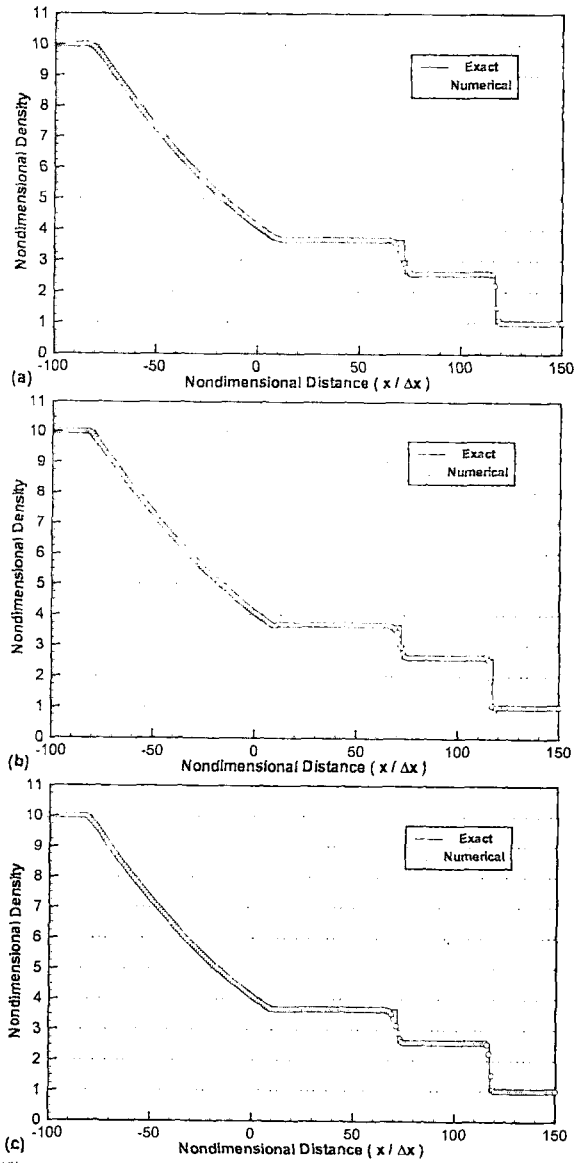

Fig. 2. Computation of shock-tube simulation (density profile) by: (a) Jameson et al.'s model, (b) Tam et al.'s model, and (c) ANAD model.

Quasi-1-D Computation

For quasi-one-dimensional transonic nozzle computations, the Problem 2 in Category 1 in the Third CAA Workshop on Benchmark Problems [16] is solved in the present study. This problem is to simulate the shock-sound interactions in a transonic nozzle. The schematic diagram of the problem is illustrated in Fig. 3. All quantities are nondimensionalized using the upstream values: length scale = D_{inlet}, density scale = ρ_{inlet}, velocity scale = c_{inlet}, pressure scale = $\rho_{inlet}c^2_{inlet}$, and time scale = D_{inlet}/c_{inlet}, where D is the nozzle height and c is the speed of sound. The domain is $-10 < x < 10$, and the area of the nozzle is given by Eq. (35). At the inflow boundary, the inlet Mach number is $M_{inlet} = 0.2006533$ and the magnitudes of acoustic perturbations are equally $\varepsilon = 1\times10^{-5}$ times of the inlet density, pressure and velocity, respectively. The frequency of perturbations is $\omega = 0.6\pi$ The mean pressure is set at the outflow boundary to create shock: $p_{exit} = 0.6071752\gamma p_{inlet}$.

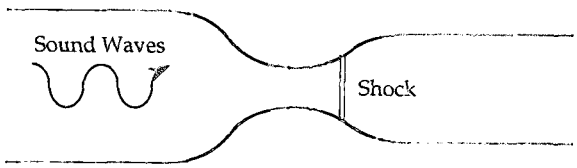

$$A(x)=\begin{cases}0.536572-0.190866\exp\left[-(\ln 2)(x/0.6)^2\right], & x>0\\ 1.0-0.661514\exp\left[-(\ln 2)(x/0.6)^2\right], & x<0\end{cases} \quad (35)$$

Fig. 3. Schematic diagram for computations of shock-sound interaction in a transonic nozzle.

For the quasi-one-dimensional computations, the equations (2) are solved. The ANAD model is used to capture the shock, remove the spurious oscillations and guide to the steady mean solutions without damping on the acoustic waves. The numbers of grid points used are 251 and the grids are clustered near the nozzle throat. The time step used is determined by CFL condition with Courant number of 0.9. The convergence criterion for steady state is that the maximum value of the residual defined as $|\rho^{(n+1)}-\rho^{(n)}|/\rho^{(n)}$ is below 1×10^{-15} which is the order of machine error. After the steady state is reached, the acoustic perturbation starts at the inlet plane, and the periodic oscillatory state with constant magnitudes is achieved during 25 wavelets are produced.

The steady mean solutions are represented in Fig. 4, where it is shown that the numerical solutions are in good agreement with the analytic solutions. The distribution of pressure perturbations ($p(x)-\bar{p}(x)$) at a start of the period of inlet perturbation are expressed in Fig. 5, where the interference between incident and reflected waves at the upstream region, the shock-sound interaction at the throat, and the transmitted waves at the downstream region are shown well. The exit pressure signal through one period is represented in Fig. 6. The results in Fig. 5 and 6 are also in good agreement with the analytic solutions that are provided by the committee of Third CAA Workshop on Benchmark Problems [16]. By the results, it is concluded that the ANAD model developed in this paper can be used accurately and effectively for unsteady CAA with the high-order and high-resolution schemes.

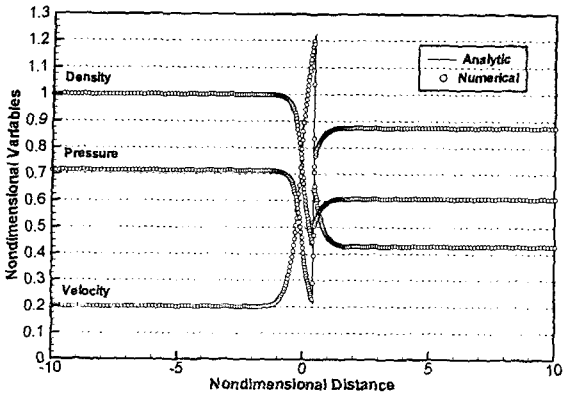

Fig. 4. Steady mean solutions compared with analytic solutions in quasi-one-dimensional transonic nozzle.

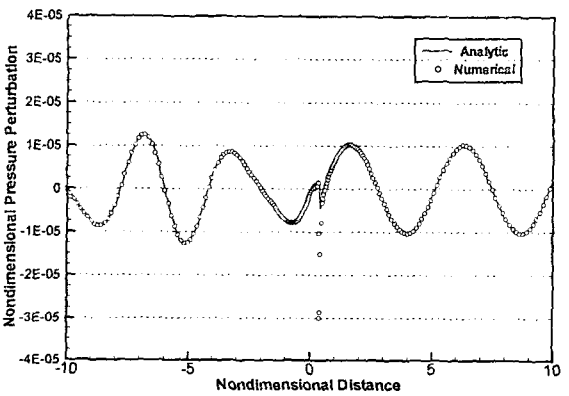

Fig. 5. Distribution of pressure perturbations at a start of the period of inlet perturbation in quasi-one-dimensional transonic nozzle.

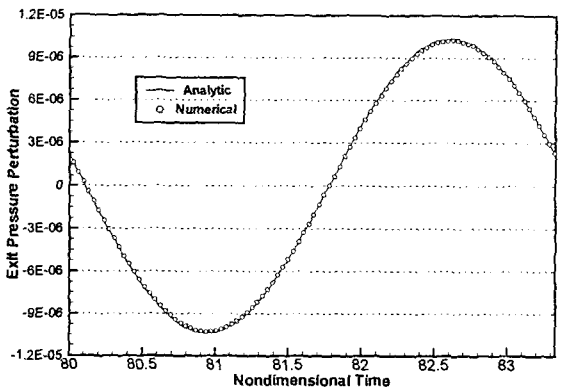

Fig. 6. Exit pressure perturbation signal through one period in quasi-one-dimensional transonic nozzle.

2-D Computation

The same problem in the previous subsection is solved in two dimensions, which is more realistic, for the validation of multi-dimensional ANAD model. For the two-dimensional transonic nozzle computations, the equations (3) are solved. The numbers of grid points used are 251 in x-direction and 25 in y-direction (251×25), where the distribution of x-directional grid points are the same as that of the quasi-one-dimensional computation. The Courant number and the convergence criterion for steady state are also the same as those of the quasi-one-dimensional computation. After the steady state is reached, the acoustic perturbation starts at the inlet plane, and the periodic oscillatory state with constant magnitudes is achieved during 25 wavelets are produced, just like the quasi-one-dimensional case.

The grid meshes are represented in Fig. 7. The contours of steady mean solutions are represented in Fig. 8. The steady mean solutions on the nozzle centerline (y = 0) are represented in Fig. 9, where it is shown that the numerical solutions are in good agreement with the analytic solutions, just as the quasi-one-dimensional results. The distribution of pressure perturbations ($p(x)-\bar{p}(x)$) on the nozzle centerline (y = 0) at a start of the period of inlet perturbation is expressed in Fig. 10, which shows no difference from the quasi-one-dimensional result of Fig. 5.

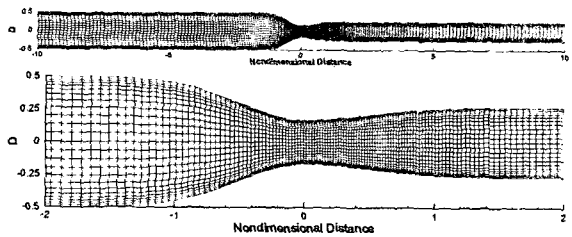

Fig. 7. Grid mesh system for two-dimensional transonic nozzle computation: entire view and zoomed view.

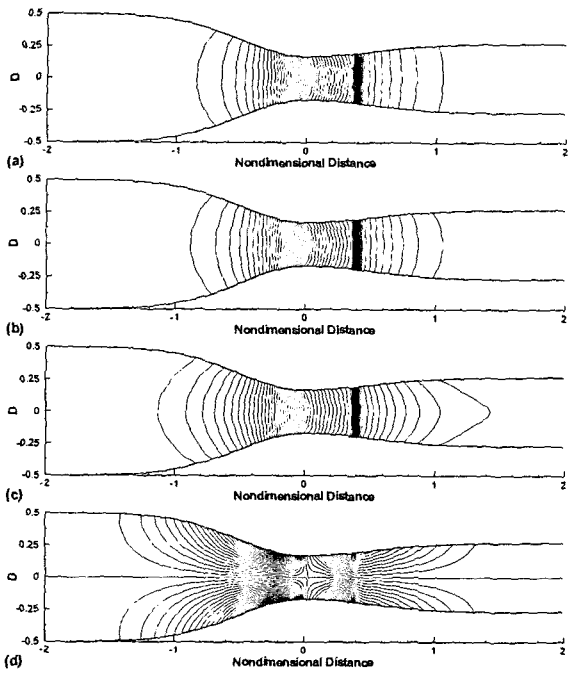

Fig. 8. Contours of steady mean solutions in two-dimensional transonic nozzle: (a) density, (b) pressure, (c) u-velocity, and (d) v-velocity.

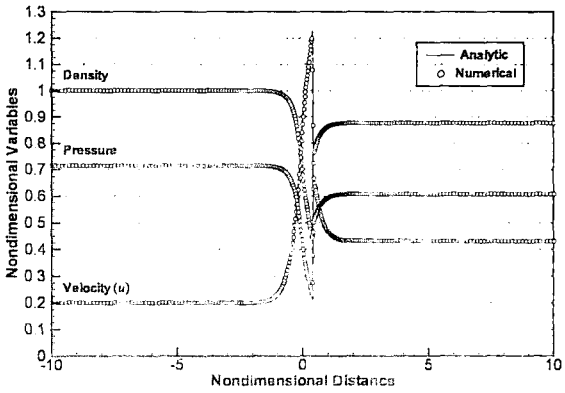

Fig. 9. Steady mean solutions compared with analytic solutions in two-dimensional transonic nozzle.

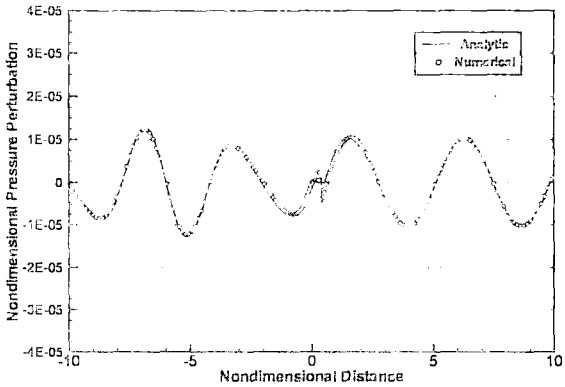

Fig. 10. Distribution of pressure perturbations at a start of the period of inlet perturbation in two-dimensional transonic nozzle.

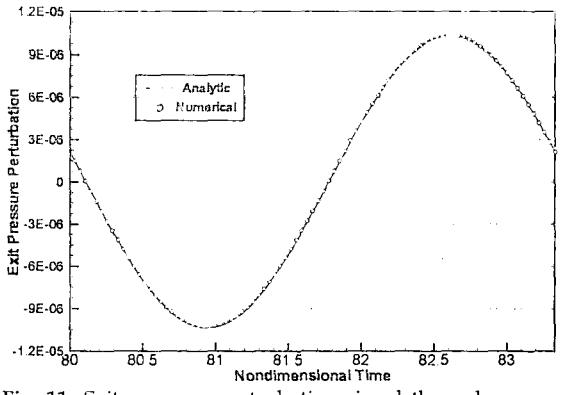

Fig. 11. Exit pressure perturbation signal through one period in two-dimensional transonic nozzle.

The exit pressure signal at the center (y = 0) through one period is represented in Fig. 11, which is also the same as that of quasi-one-dimensional result of Fig. 6. Therefore, it is concluded that the ANAD model developed in this paper can be used accurately and effectively for the multi-dimensional unsteady CAA with the high-order and high-resolution schemes.

VI. Conclusions

Adaptive nonlinear artificial dissipation (ANAD) model is presented for the numerical stability and convergence of CAA with high-order and high-resolution schemes. The ANAD model has effective shock-capturing features with excellent background smoothing but it scarcely dissipates the linear acoustic waves. It has the adaptive control constant to determine the optimum value of overall dissipation magnitude automatically according to the problem types and flow conditions, so it is not needed anymore to waste additional time for trial and error in searching proper value of the constant. The one-, quasi-one- and two-dimensional formulations of the ANAD model are successfully accomplished and their applications to the actual Euler computations of benchmarking problems provide the high-quality nonlinear shock and linear acoustic wave solutions.

References

1. Kim, J. W., and Lee, D. J., *AIAA Journal*, Vol. 34, No. 5, 1996, pp. 887-893.
2. Kim, J. W., and Lee, D. J., *Computational Fluid Dynamics Journal*, Vol. 5, No. 3, 1996, pp. 281-300.
3. Kim, J. W., and Lee, D. J., *Journal of Computational Acoustics*, Vol. 5, No. 2, 1997, pp. 177-191.
4. Tam, C. K. W., AIAA Paper 95-0677.
5. Jameson, A., *Numerical Methods in Aeronautical Fluid Dynamics*, New York, Academic Press, 1982, pp. 289-308.
6. Pulliam, T. H., AIAA Paper 85-0438.
7. Jameson, A., Schmidt, W., and Turkel, E., AIAA Paper 81-1259.
8. Pulliam, T. H., and Steger, J. L., AIAA Paper 85-0360.
9. Swanson, R. C., and Turkel, E., AIAA Paper 87-1107.
10. Tam, C. K. W., Webb, J. C., and Dong, Z., *Journal of Computational Acoustics*, Vol. 1, No. 1, 1993, pp. 1-30.
11. Tam, C. K. W., and Shen, H., AIAA Paper 93-4325.
12. Tam, C. K. W., and Webb, J. C., *Journal of Computational Physics*, Vol. 107, 1993, pp. 262-281.
13. Thompson, K. W., *Journal of Computataional Physics*, Vol. 89, 1990, pp. 439-461.
14. Poinsot, T. J., and Lele, S. K., *Journal of Computational Physics*, Vol. 101, 1992, pp. 104-129.
15. Kim, J. W., and Lee, D. J., *AIAA Journal*, Vol. 38, No. 11, 2000, pp. 2040-2049.
16. Kim, J. W., and Lee, D. J., Proceedings of Third CAA Workshop on Benchmark Problems, NASA/CP-2000-209790, pp. 235-245.